chemosensors

MDPI

Article

Engineering Raspberry-like Plasmonic Nanoclusters as Tags in Surface-Enhanced Raman Scattering-Based Immunoassays

Jingwen Xu, Shizhen Huang, Zhida Gao and Yanyan Song *

College of Sciences, Northeastern University, Shenyang 114001, China
* Correspondence: yysong@mail.neu.edu.cn

Abstract: Surface-enhanced Raman scattering (SERS) is highly attractive with the advantages of non-destructive performance, high specificity, and ultra-sensitivity. However, it is still a great challenge to design SERS tags with strong and undisturbed SERS signals via a simple method for an SERS-based immunoassay. Herein, a simple one-pot method was developed for the fabrication of SERS nanotags with interior reporters located at the nanogaps between plasmonic structures. Benefiting from the reducibility and easy-to-polymerize properties of aniline, Au^{3+} ions were reduced and grew into small-sized Au nanoparticles with a thin layer of polyaniline (PANI) by using aniline as the reductant. Following the continuous polymerization and the reduction reactions, PANI-coated Au nanoparticles were assembled into a nanocluster with sub 5 nm gaps, and PANI located at these gaps were used as interior reporters in SERS tags. As proof-of-concept, a histidine-tagged antigen was used as the model analyte for the SERS-based immunoassay. The proposed sensing platform showed the response to the histidine-tagged antigen ranging from 0.1 to 1000 ng mL^{-1} with a detection limit of 0.01 ng mL^{-1}. The remarkable and undisturbed SERS signals make the proposed SERS tags feasible for detections of biomarkers with a low concentration in complex biological samples.

Keywords: one-pot method; plasmonic nanostructure; SERS tags; immunoassay

check for updates

Citation: Xu, J.; Huang, S.; Gao, Z.; Song, Y. Engineering Raspberry-like Plasmonic Nanoclusters as Tags in Surface-Enhanced Raman Scattering-Based Immunoassays. *Chemosensors* **2022**, *10*, 442. https://doi.org/10.3390/chemosensors10110442

Academic Editors: Shan Cong and Chunlan Ma

Received: 29 September 2022
Accepted: 24 October 2022
Published: 26 October 2022

Publisher's Note: MDPI stays neutral with regard to jurisdictional claims in published maps and institutional affiliations.

Copyright: © 2022 by the authors. Licensee MDPI, Basel, Switzerland. This article is an open access article distributed under the terms and conditions of the Creative Commons Attribution (CC BY) license (https://creativecommons.org/licenses/by/4.0/).

1. Introduction

Surface-enhanced Raman scattering (SERS) has emerged as an alternative analytical technique owing to its ultrahigh sensitivity and non-destructive performance providing chemical fingerprints for analytes [1–4]. Moreover, SERS technology is highly competent for directly identifying biological molecules in lia quid medium, which is an insuperable challenge for other detection technologies [5–8]. Combined with immunoassays, SERS has been applied to high-throughput and trace detection of various biomarkers, exhibiting great potential in the early diagnosis of diseases. [9–11] Generally, a SERS-based immunoassay relies on an antibody-functionalized SERS tags, which can selectively recognize and localize the target protein [12,13]. Unlike the enzyme or fluorescein in traditional immunoassay technology, a SERS tag is less expensive and more stable, and the signal of the SERS tag can be read directly and rapidly [14–16]. Since most targeted antigens are present with low abundance in samples, it is crucial to design highly sensitive SERS tags to ensure detectable signals.

The key component of a SERS tag is the plasmonic nanostructure with a light-induced localized electromagnetic field, which can provide million-fold enhanced signals for reporter molecules [17,18]. Therefore, the fabrication of the SERS substrate with increased electromagnetic field enhancement is of great significance. Both theoretical and experimental studies have shown that the electromagnetic field in sharp tips or nanogaps in concrete areas can be increased by multiple orders of magnitude [19–21]. The SERS substrates with hybrid configurations or anisotropic nanostructures such as core–shell structure [22,23], nanoclusters [24,25], and satellite structures [26] have already been demonstrated to yield much higher SERS activities than isolated spherical nanoparticles. For these nanostructures, efficient interparticle plasmonic couplings in nanostructures can provide abundant

"hot spots" with high electromagnetic enhancement [27,28]. With regard to the shape of the nanostructure, much effort has been dedicated to design of sensitive SERS tags for SERS-based immunoassays. For example, Jun's group fabricated Ag–Au bimetallic SERS tags with abundant hot spots by controlling the growth of Ag shells on Au nanostructures immobilized on silica core particles, allowing the sensitive detection of antigens in concentrations as low as 0.09 ng/mL [10]. Wang et al. designed core-satellite nanostructures as SERS tags for immunoassays, exhibiting remarkable SERS activity for antigen detection [29]. In general, the current synthesis of these SERS tags involves at least a two-step route: preparation of plasmonic nanostructures and assembly of subsequent reporter molecules [30]. With the success in sensitivity and specificity, the application of SERS tags still faces several challenges: (i) complex and time-consuming procedures are required to fabricate plasmonic nanostructure with high SERS activity; (ii) the competitive adsorption of undesired sulfhydryl containing protein in a biological sample on the surface of a metal nanostructure may interfere with the connection between the reporter molecules and metal nanoparticles, causing a decrease in the signal intensity of the reporter molecules; and (iii) engineering "hot spots" with high reproducibility is still challenging, and thus largely impacts the reliability of SERS-based immunoassay technology.

To address these issues, herein, we present a simple one-pot approach to fabricate polymer-functionalized Au nanoclusters (pAuNCs) as SERS tags. The pAuNCs were prepared by the reduction of chloroauric acid with aniline as the reductant at room temperature. In addition to reduction, aniline molecules simultaneously polymerized into polyaniline (PANI) at the surface of Au nanoparticles in an acidic environment, and then PANI-coated Au nanoparticles assembled into a nanocluster with continuous polymerization reactions. Particularly, the thin PANI layer helped form sub-5 nm gaps between the neighboring Au nanoparticles as hot spots, providing large electric fields for enhanced Raman scattering. Since the PANI molecules in these gaps exhibit excellent SERS signals, the pAuNCs were successfully used as the SERS tags for immunoassays. As a proof-of-concept, prostate-specific antigen (PSA) was detected by the proposed SERS platform via a specific antigen–antibody interaction. Because the PSA level of older males is abnormal when prostatitis, prostate hyperplasia, and prostate cancer occur in the prostate, PSA is considered as an organ-specific biomarker for diagnosis and prognosis of prostate-related diseases [31,32]. To the best of our knowledge, this is the first study demonstrating the synthesis of SERS tags by the one-pot method without the use of extra reporter molecules. Because of the uniform and compact coverage of PANI on Au nanoparticles, the pAuNCs showed considerable SERS activities with high repeatability and anti-interference capability.

2. Materials and Methods

2.1. Chemicals and Materials

Sodium acetate, aniline, chloroauric acid ($HAuCl_4 \cdot 4H_2O$), NaH_2PO_4, Na_2HPO_4, nickel chloride ($NiCl_2 \cdot 6H_2O$), sodium acetate, isopropanol, and ethanol were purchased from Sinopharm Chemical Reagent Co., Ltd. (Shanghai, China). Bovine serum albumin (BSA) and triton-100 were obtained from Sigma-Aldrich (St. Louis, MO, USA). His-tagged antigens (KLK3) and corresponding antibodies were purchased from Sangon Biotech Co., Ltd. (Shanghai, China). All these reagents were of analytical grade or higher and used as received without further purification. Deionized (DI) water was used to prepare all solutions.

2.2. Synthesis of Raspberry-like pAuNCs

Raspberry-like pAuNCs were synthesized through a simple one-pot method. First, 0.82 g of sodium acetate was dissolved in 17 mL of DI water, followed by the immediate addition of a mixture of 50 µL aniline and 300 µL TritonX-100. A uniform emulsion thus formed after continuous stirring for 15 min. Then, 2 mL of $HAuCl_4$ (1%) was added into the emulsion, and the mixture was intensely stirred for another 30 s to ensure complete mixing. Finally, the resulted solution was left at 4 °C for a period and then centrifuged at

12,000× *g* rpm for 5 min. The precipitate thus obtained was then dispersed with DI water and stored at 4 °C.

2.3. Modification of Antibody on pAuCNs

First, 12.5 μL of antibody (0.8 mg mL^{-1}) was added into 250 μL of colloidal pAuCNs solution (5.7 mg/mL) and gently stirred at 4 °C for 12 h. The antibody-modified pAuCNs were collected by centrifugation at 12,000× *g* rpm for 5 min. Then, the resulting antibody-modified pAuCNs were resuspended in 2 mL of BSA solution (1 wt%) at 4 °C for 2 h to block the unreacted and non-specific sites on pAuCNs.

2.4. Synthesis of Substrate for Antigen Capture

$Ni(OH)_2/TiO_2$ film substrate was synthesized to capture the histidine-containing antigen. First, the TiO_2 film was fabricated by an anodic oxidation process, using a two-electrode system with a platinum plate as the counter electrode and Ti foil as the working electrode. After ultrasonic cleaning, the Ti foil was anodized in an electrolyte of 1.0 M H_2SO_4 at 20 V for 30 min to form the TiO_2 film, and the TiO_2 film was then annealed in air at 450 °C for 2 h. The deposition of $Ni(OH)_2$ was performed by an electrochemical method in a three-electrode cell with a saturated calomel electrode (SCE) as the reference electrode, a platinum plate as the counter electrode, and the as-prepared TiO_2 film as the working electrode [33]. The electrodeposition of metallic nickel was conducted in an aqueous solution containing 20 mM nickel chloride at a constant potential of −0.9 V for 600 s. Afterwards, the nickel deposited on TiO_2 film was oxidized in a 0.1 M NaOH solution by cyclic voltammetry scanning in the potential ranging from 0.1 to 0.7 V and a scan rate of 50 mV s^{-1} for 25 cycles.

2.5. Procedure of the SERS-Based Immunoassay

The $Ni(OH)_2/TiO_2$ film was first immersed in different concentrations of antigen (30 μL, 0.1 M phosphate buffered saline (PBS), pH 7.4). After incubating at 4 °C for 12 h, the $Ni(OH)_2/TiO_2$ films were washed with PBS thoroughly. Then, antibody modified pAuCNs (30 μL) were added onto the films and incubated at 4 °C for another 2 h. Next, the $Ni(OH)_2/TiO_2$ film was rinsed with PBS solution and DI water and dried for SERS measurements.

2.6. SERS Detection

SERS measurements were performed using a Raman microscope (LabRAM HR, HORIBA Scientific, Palaiseau, France) with a laser excited at 785 nm. The sample was observed through a 50 × objective lens with a 1 μm spot size. The laser power was 15 mW, and integration time for each spectrum was 1 s; the confocal hole was 200 μm, and the slit aperture was 300 μm. Data acquisition was performed with three accumulations, and the spectrometer was calibrated using the Raman spectra of silicon wafer at 520.7 cm^{-1}. All the spectra were collected at three different points for each sample, and the Raman intensity at 1161 cm^{-1} was calculated according to the average intensity of the three points.

2.7. Finite-Difference Time-Domain (FDTD) Simulation of Au Nanocluster

The FDTD method was used to simulate the electromagnetic field enhancement of the pAuNCs nanostructures. The pAuNCs nanostructures model were composed of several Au nanoparticles covered by a PANI layer with a 3 nm thickness. An Au nanoparticle with a diameter of 8 nm is then stacked into a nanocluster structure with a diameter of about 50 nm to match the actual structure, according to the related TEM images (Figure S1), and the wavelength was set to be 785 nm in the FDTD simulation.

2.8. Instrumentation

The UV-vis absorption spectra were recorded by a Perkin-Elmer spectrometer (Lambda 750S, Waltham, MA, USA). Transmission electron microscopic (TEM) and high-resolution

TEM (HR-TEM) images were taken on a transmission electron microscope (JEOL 2000, Tokyo, Japan). Scanning electron microscopy (SEM) experiments were carried out using a SEM SU 8000 microscope (Hitachi, Tokyo, Japan) at an accelerating voltage of 5 kV. The electrochemical signals were collected on a CHI 660E electrochemical workstation.

3. Results and Discussion

3.1. Fabrication and Characteristics of Raspberry-like pAuNCs

For the fabrication of the raspberry-like pAuNCs, Au^{3+} ions in $HAuCl_4$ were first reduced into Au^0, forming undersized Au nanoparticles with the reduction of aniline. As shown in Figure 1A, Au nanoparticles grew continuously along with the iterative reduction, and aniline was simultaneously polymerized into PANI under an acidic solution. Consequently, a thin and compact PANI layer coated on the Au nanoparticle formed, further giving rise to the aggregation of Au nanoparticles into the nanocluster. The plasmonic nanoclusters were obtained by the one-pot method within 30 min, using no additional polymerizing agent. The morphology and structure of the raspberry-like pAuNCs were characterized by TEM. Figure 1B and Figure S1 show the raspberry-like pAuNCs with an average diameter of ~50 nm, comprising several Au nanoparticles (~8 nm). As shown in Figure 1C, the gaps with ~3 nm were observed between Au nanoparticles in pAuNCs. The gap structure is well known to support a strong electric field localization and can induce enhanced Raman scattering of the molecules in gaps [28].

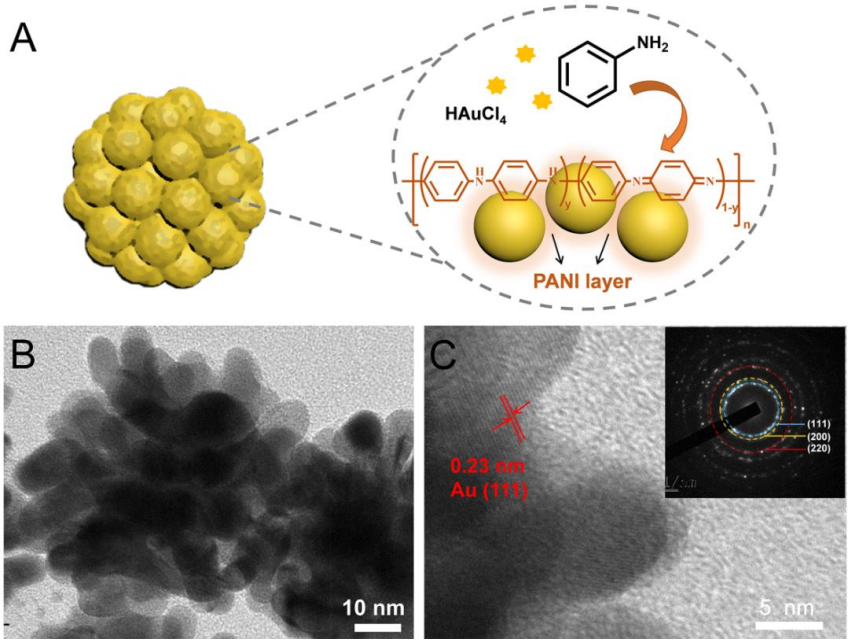

Figure 1. (**A**) Schematic illustration of $HAuCl_4$ reduction by aniline to fabricate raspberry-like pAuNCs. (**B**) TEM and (**C**) HR-TEM images of the pAuNCs (inset: SAED image of pAuNCs).

Integration time is also a vital factor affecting the morphology and SERS activity of pAuNCs. The SEM images in Figure S2 show that the size of Au nanoparticles increased with reaction time, and Au nanoparticles coated with a PANI layer were incorporated into a larger nanocluster. With excess aniline, nanoclusters continuously germinated, and the size of pAuNCs was ~200 nm at 30 min reaction time (Figure S2D). However, pAuNCs with a reaction time of 30 min showed decreased SERS activity (Figure S3), and this may be ascribed to the thick PANI layer over Au nanoparticles. Since a longer reaction time can result in further polymerization, the gap sizes between neighboring Au nanoparticles in nanoclusters increased, thus leading to weak electromagnetic fields. The reaction time was thus optimized as 10 min according to the SERS performance of pAuNCs, and the aniline concentration was chosen as 50 μL (Figure S4). The HR-TEM image of the pAuNCs

in Figure 1C shows the lattice spacing of Au as 0.23 nm, and the selected-area electron diffraction (SAED) image further confirms the (111), (200), and (220) crystal planes of the face-centered cubic Au crystals. The coverage of PANI was verified by the FT-IR spectrum (Figure S5). Distinct peaks located at 1292, 1512, and 1612 cm^{-1} can be ascribed to the characteristic C–N stretching vibration mode, N–B–N, and N = B = N deformation of the polyaniline, respectively [34]. The EDS analysis further confirmed the presence of Au, C, and N elements in pAuNCs (Figure S6).

3.2. SERS Performance of the pAuNCs

The UV–vis spectra of the pAuNCs are shown in Figure 2A. Obvious absorption peaks at ~230 nm and ~290 nm are assigned to the PANI in pAuNCs. Meanwhile, the wide absorption peak at ~550 nm is attributed to the surface plasmon resonance (SPR) of Au nanoparticles. The dependence of the SERS intensity on the laser excitation wavelength was investigated by employing a laser at 532, 633, and 785 nm. As shown in Figure S7, the SERS signal obtained with 785 nm was the strongest, and thus SERS studies were carried out using the excitation line at 785 nm. Raman spectra of the raspberry-like pAuNCs were acquired using a laser excited at 785 nm and are shown in Figure 2B. The Raman spectrum of pAuNCs showed obvious peaks at 518, 1161, 1219, 1481, and 1661 cm^{-1}, attributed to the ring deformation, δ(C−H), ν(C−N), ν(C = N), and ν(C = C) of PANI molecules, respectively. The intense Raman signals can be attributed to the sufficient polymerization of aniline during our approach. During the one-pot fabrication process, Au^{3+} ions are reduced by aniline into Au nanoparticles, and the aniline molecules are simultaneously polymerized into PANI at the surface of Au nanoparticles in an efficient manner. Au nanoparticles were assembled by these thin PANI layers, thus forming clusters with the PANI layers of ~3 nm thickness between neighboring Au nanoparticles. Since the plasmon coupling between Au nanoparticles in very close proximity can generate strong electric fields, the PANI located at the interparticle junctions exhibit strong SERS signals.

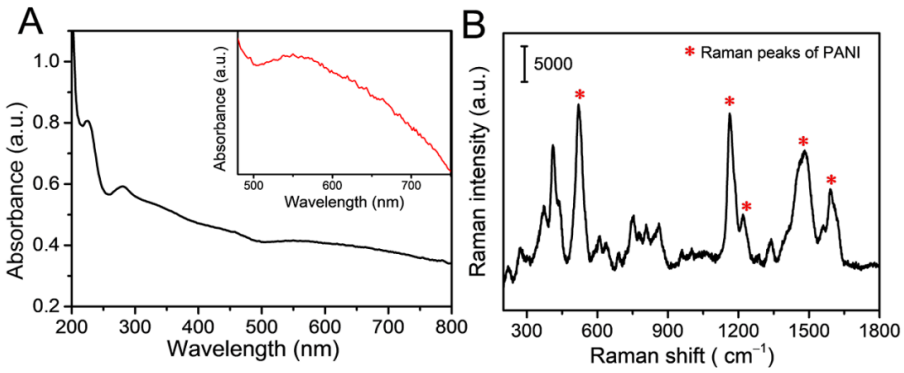

Figure 2. (**A**) UV–vis absorption spectra. (**B**) Raman spectrum of the pAuNCs (* indicated the Raman peaks of PANI).

To visualize the electric field distribution and intensity, the enhanced electric fields of raspberry-like pAuNCs were simulated using 3D finite-difference time-domain (FDTD) according to the TEM images of pAuNCs shown in Figure 3A. Figure 3B shows the calculated contours of $|E/E_0|^2$, where E and E_0 are the amplitude of the enhanced and incident electric fields, respectively. The narrow gaps in pAuNCs show strong electric fields (red colored regions). Nanocluster structure can provide multiple hot spots with an enhanced electric field, resulting in the enhanced Raman scattering for reporter molecules located at the hot spots. Owing to the high Raman intensity of PANI in nanoclusters, the proposed pAuNCs were then used as the SERS tags, whereas the PANI acted as the reporter.

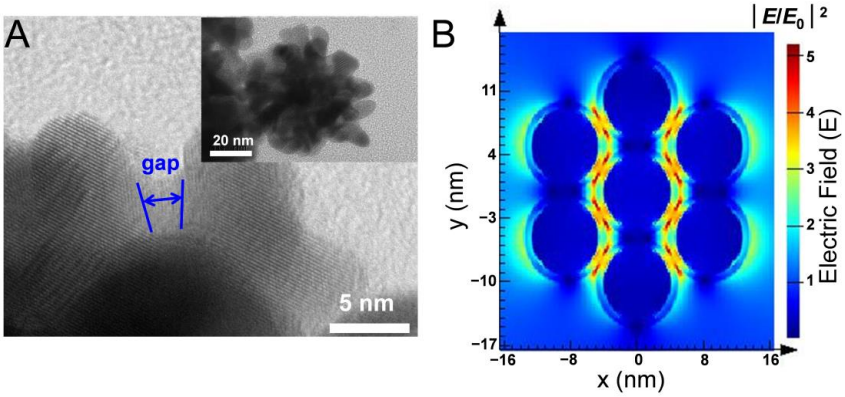

Figure 3. (**A**) TEM images and (**B**) electric field by FDTD simulation of the pAuNCs.

To verify the feasibility of the prepared pAuNCs as SERS tags for quantitative immunoassays, SERS spectra of pAuNCs in different concentrations were recorded and shown in Figure 4A. For the concentration of pAuNCs ranging from 0.001 to 10.0 mg L^{-1}, the intensity of SERS peaks increased with higher amounts of SERS tags. The Raman peaks of pAuNCs at 518, 1168, and 1661 cm^{-1} show an obvious upward tendency along with the increased pAuNCs concentrations (Figure 4B). Meanwhile, a reasonable corresponding relationship was observed between the pAuNCs concentration and the intensity of the peak at 1168 cm^{-1} with a correlation coefficient (R^2) of 0.982 (Figure S8 of the Supporting Information). The good correlation between the concentration of pAuNCs and SERS intensity confirmed the feasibility of the raspberry-like pAuNCs as the SERS tags for performing quantitative assays. Since the signal uniformity is an important factor determining the suitability of SERS tags for practical applications, SERS spectra of pAuNCs were collected on 10 random spots to evaluate the signal reproducibility of the prepared pAuNCs. Uniform Raman spectra of pAuNCs from these spots can be observed in Figure 4C, and the relative standard deviation (RSD) of the Raman peak at 1168 cm^{-1} was determined to be 4.86% (Figure 4D), indicating a satisfactory uniformity of the prepared pAuNCs as SERS tags for further applications.

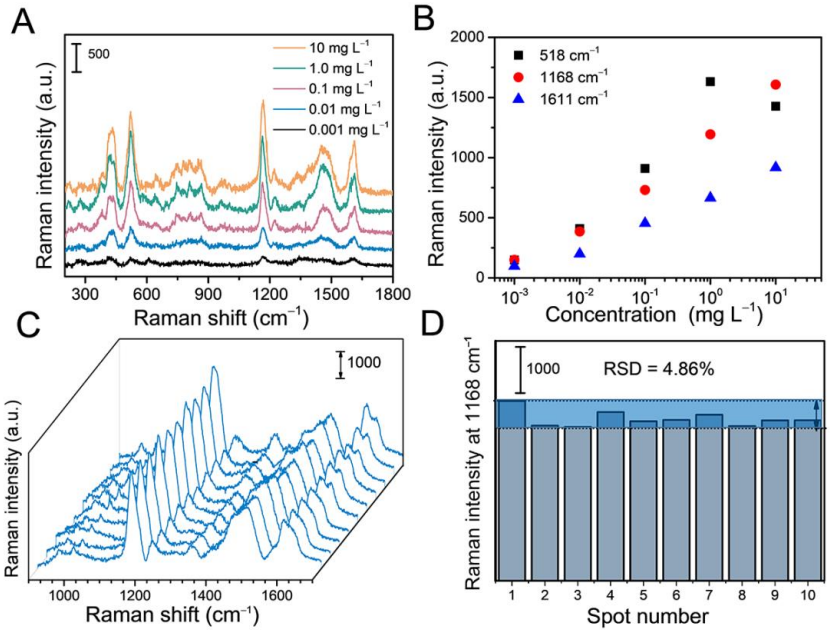

Figure 4. (**A**) SRES spectra of pAuNCs with different concentrations and (**B**) the corresponding signal intensity at 518, 1168, and 1661 cm^{-1}. (**C**) SERS spectra of pAuNCs collected from 10 random spots and (**D**) the corresponding signal intensity at 1168 cm^{-1}.

3.3. Evaluation of the SERS-Based Immunoassay

For proof-of-concept in a SERS-based immunoassay, the pAuNCs were applied as SERS tags to detect a cancer-related biomarker (prostate-specific antigen, PSA). As shown in Figure 5A, PSA with histidine tags (his-tagged PSA) was first captured on a Ni(II) contained substrate and then detected by the SERS tags via immune recognition. Prior to detection, the pAuNCs were conjugated to the corresponding antibodies for immune recognition of the target antigen. After the conjugation of antibodies on pAuNCs, the SERS signal did not show any discernible change when compared to the pristine SERS tags (blue line, Figure 5B). Since the gaps in pAuNCs were filled with a polymer layer, antibodies or other interferences in the sample are not allowed to approach hot spots in SERS tags, and interference-free SERS signals can be obtained from the raspberry-like pAuNCs. The interference-free SERS tags were then applied as an interior reporter- marked nanotag for further SERS detection.

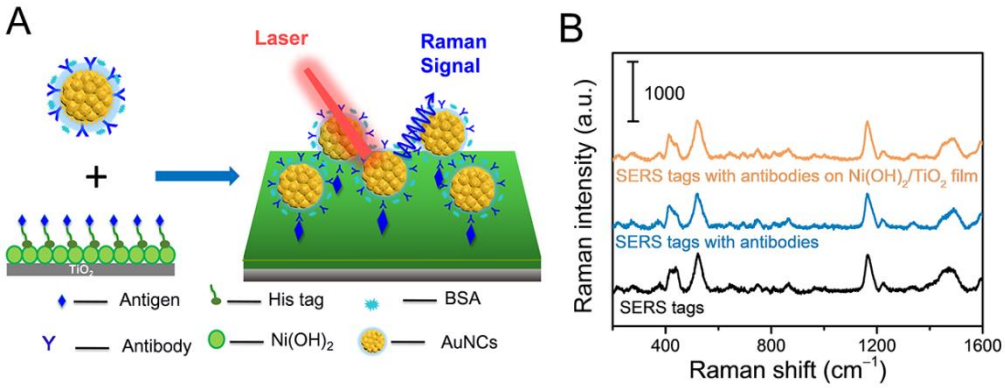

Figure 5. (**A**) Schematic diagram of SERS-based immunosensor for his-tagged antigen detection. (**B**) SERS spectra of SERS tags with different modifications.

As shown in Figure 5A, his-tagged PSA was first captured on the $Ni(OH)_2/TiO_2$ film via affinity interaction between Ni(II) and histidine, and this method has been widely used for the extraction and stabilization of biomolecules containing histidine [35]. To capture the his-tagged protein, the Ni^{2+}-containing substrate was fabricated by coating a layer of nickel hydroxide on a TiO_2 film via a simple electrochemical deposition (Figure S9). The TiO_2 film was used as a low-cost and recyclable electrode for Ni^{2+} deposition [36]. The morphology and structure of the $Ni(OH)_2/TiO_2$ film were characterized by SEM image and EDS analysis in Figure S10. The $Ni(OH)_2/TiO_2$ film substrate did not have an influence on the SERS signals of pAuNCs (Figure S11). Then, the SERS tags conjugated with antibodies were connected to the antigens on the film via immune recognition, and the concentration of antigens was determined by the amount of the SERS tags. Particularly, the signals of SERS tags were still undisturbed after incubation on the $Ni(OH)_2/TiO_2$ film (Figure 4B), indicating the potential of the prepared SERS tags for detection in complex environments.

To evaluate the analytical performance of the proposed SERS-based sensing platform, his-tagged PSA with different concentrations were detected. After capturing by the $Ni(OH)_2/TiO_2$ substrate, the antigens then bonded with antibodies on SERS tags via immune interaction. Antigens in higher concentrations can bond with more SERS tags, thus resulting in more intense SERS signals. As we expect, the SERS signal intensity of SERS tags increased with increasing concentration of his-tagged PSA (Figure 6A). As shown in Figure 6B, a linear curve was established by plotting the SERS peak intensity at 1168 cm^{-1} against the concentrations of his-tagged PSA ranging from 0.1 to 1000 ng mL^{-1}. In addition, the linear equation in Figure 6B was calculated as $y = 185.1 + 111.06 \times \log C$ with an R^2 of 0.9973, and the limit of detection (LOD) was 0.01 ng mL^{-1}, estimated from the signal-to-noise ratio of three measurements. To prove the capture of the $Ni(OH)_2$ towards his-tagged antigens, the detection of his-tagged PSA was also carried on a TiO_2 film instead

of a $Ni(OH)_2/TiO_2$ film, and there was no linear relationship between the SERS intensity and antigen concentrations (Figure S12).

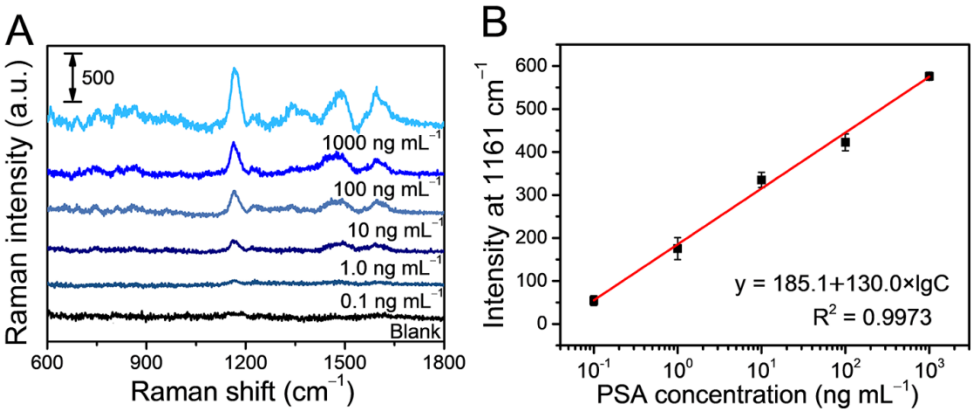

Figure 6. (**A**) SERS spectra of pAuNCs incubated with different concentrations of his-tagged antigen on $Ni(OH)_2/TiO_2$ films. (**B**) The calibration curve of the intensity of SERS signals at 1161 cm^{-1} versus the concentration of his-tagged antigen.

4. Conclusions

In summary, a SERS tag was prepared by the one-pot synthetic method, using PANI as the SERS reporter located at the gaps of the Au nanocluster. Benefiting from strong electric fields produced by the plasmon coupling between Au nanoparticles in very close proximity, the prepared SERS nanotags provided a remarkable and undisturbed signal for a SERS-based immunoassay. For proof-of-concept, the detection of his-tagged PSA ranging from 0.1 ng mL^{-1} to 1000 ng mL^{-1} was achieved with an LOD of 0.01 ng mL^{-1}. Furthermore, through the modification of different antibodies or aptamers, the SERS tags can be easily extended for detecting a diverse range of diseased-related biomarkers, including antigens and nucleic acid in complex biological samples.

Supplementary Materials: The following supporting information can be downloaded at: https://www.mdpi.com/article/10.3390/chemosensors10110442/s1, Figure S1: TEM image of pAuNCs; Figure S2: SEM images of pAuNCs with different reaction times (A) 30 s, (B) 1 min, (C) 10 min, and (D) 30 min; Figure S3: SERS spectra of pAuNCs with different reaction times; Figure S4: SERS spectra of pAuNCs with different aniline concentrations; Figure S5: FT IR spectrum of p AuNCs; Figure S6: EDS analysis of pAuNCs; Figure S7: SERS spectra of pAuNCs under different laser excitation wavelength; Figure S8: The calibration curve of the intensity of SERS signals at 1168 cm^{-1} versus the concentration of pAuNCs; Figure S9: CV curves of $Ni(OH)_2/TiO_2$ film in 0.1 M NaOH between 0.1 and 0.7 V at a scan rate of 50 mV s^{-1} for 25 cycles; Figure S10: (A) SEM image and (B) EDS spectra of $Ni(OH)_2/TiO_2$ film; Figure S11: SERS spectra of pAuNCs on different glass, TiO_2 film, and $Ni(OH)_2$ /TiO_2 film as substrate; Figure S12: SERS spectra of pAuNCs incubated with different concentrations of his-tagged antigen on TiO_2 films.

Author Contributions: Conceptualization, J.X. and S.H.; methodology, S.H.; validation, Z.G.; writing—review and editing, Y.S. All authors have read and agreed to the published version of the manuscript.

Funding: This research was funded by the National Natural Science Foundation of China (grants nos. 22204016, 22074013, and 21874013), and the Fundamental Research Funds for the Central Universities (grants nos. N2105018, N2205005, and N2005027).

Institutional Review Board Statement: Not applicable.

Informed Consent Statement: Not applicable.

Data Availability Statement: The data presented in this study are available on request from the corresponding author. The data are not publicly available due to privacy.

Conflicts of Interest: The authors declare no conflict of interest.

References

1. Bell, S.E.J.; Charron, G.; Cortés, E.; Kneipp, J.; Chapelle, M.L.; Langer, J.; Procházka, M.; Tran, V.; Schlücker, S. Towards reliable and quantitative surface-enhanced Raman scattering (SERS): From key parameters to good analytical practice. *Angew. Chem. Int. Ed.* **2020**, *59*, 5454–5462. [CrossRef] [PubMed]
2. Huang, J.; Mousavi, M.Z.; Giovannini, G.; Zhao, Y.; Hubarevich, A.; Soler, M.A.; Rocchia, W.; Garoli, D.; Angelis, F.D. Multiplexed discrimination of single amino acid residues in polypeptides in a single SERS hot spot. *Angew. Chem. Int. Ed.* **2020**, *59*, 11423–11431. [CrossRef] [PubMed]
3. Song, G.; Cong, S.; Zhao, Z. Defect engineering in semiconductor-based SERS. *Chem. Sci.* **2022**, *13*, 1210. [CrossRef]
4. Li, J.; Yan, H.; Tan, X.; Lu, Z.; Han, H. Cauliflower-inspired 3D SERS substrate for multiple mycotoxins detection. *Anal. Chem.* **2019**, *91*, 3885–3892. [CrossRef] [PubMed]
5. Shi, C.; Zheng, B.; Li, J.; Zhou, Y.; Liu, H.; Ahmed, S.A.; Wang, K.; Xia, X. Three-dimensional metamaterial for plasmon-enhanced Raman scattering at any excitation wavelengths from the visible to near-infrared range. *Anal. Chem.* **2021**, *93*, 1409–1415. [CrossRef] [PubMed]
6. Oner, I.; Querebillo, C.; David, C.; Gernert, U.; Walter, C.; Driess, M.; Leimkuhler, S.; Ly, K.; Weidinger, I. High electromagnetic field enhancement of TiO_2 nanotube electrodes. *Angew. Chem. Int. Ed.* **2018**, *57*, 7225–7229. [CrossRef] [PubMed]
7. Xu, J.; Xue, Y.; Jian, X.; Zhao, Y.; Dai, Z.; Xu, J.; Gao, Z.; Mei, Y.; Song, Y.-Y. Understanding of chiral site-dependent enantioselective identification on a plasmon-free semiconductor based SERS substrate. *Chem. Sci.* **2022**, *13*, 6550–6557. [CrossRef]
8. Yang, L.; Feng, J.; Wang, J.; Gao, Z.; Xu, J.; Mei, Y.; Song, Y. Engineering large-scaled electrochromic semiconductor films as reproductive SERS substrates for operando investigation at the solid/liquid interfaces. *Chin. Chem. Lett.* **2022**, *33*, 5169–5173. [CrossRef]
9. Camacho, S.A.; Sobral-Filho, R.G.; Aoki, P.H.B.; Constantino, C.J.L.; Brolo, A.G. Zika immunoassay based on surface-enhanced Raman scattering nanoprobes. *ACS Sens.* **2018**, *3*, 587–594. [CrossRef]
10. Pham, X.; Hahm, E.; Kim, T.H.; Kim, H.-M.; Lee, S.H.; Lee, S.C.; Kang, H.; Lee, H.-Y.; Jeong, D.H.; Choi, H.S.; et al. Enzyme-amplified SERS immunoassay with Ag-Au bimetallic SERS hot spots. *Nano Res.* **2020**, *13*, 3338–3346. [CrossRef]
11. Yang, Y.; Zhu, J.; Weng, G.-J.; Li, J.-J.; Zhao, J.-W. Gold nanoring core-shell satellites with abundant built-in hotspots and great analyte penetration: An immunoassay platform for the SERS/fluorescence-based detection of carcinoembryonic antigen. *Chem. Eng. J.* **2021**, *409*, 128173. [CrossRef]
12. Yin, Y.; Li, Q.; Ma, S.; Liu, H.; Dong, B.; Yang, J.; Liu, D. Prussian blue as a highly sensitive and background-free resonant Raman reporter. *Anal. Chem.* **2017**, *89*, 1551–1557. [CrossRef] [PubMed]
13. Li, T.-D.; Zhang, R.; Chen, H.; Huang, Z.-P.; Ye, X.; Wang, H.; Deng, A.-M.; Kong, J.-L. An ultrasensitive polydopamine bi-functionalized SERS immunoassay for exosome-based diagnosis and classification of pancreatic cancer. *Chem. Sci.* **2018**, *9*, 5372–5382. [CrossRef] [PubMed]
14. Yuan, K.; Mei, Q.; Guo, X.; Xu, Y.; Yang, D.; Sánchez, B.J.; Sheng, B.; Liu, C.; Hu, Z.; Yu, G.; et al. Antimicrobial peptide based magnetic recognition elements and Au@Ag-GO SERS tags with stable internal standards: A three in one biosensor for isolation, discrimination and killing of multiple bacteria in whole blood. *Chem. Sci.* **2018**, *9*, 8781–8795. [CrossRef] [PubMed]
15. Khlebtsov, B.N.; Bratashov, D.N.; Byzova, N.A.; Dzantiev, B.B.; Khlebtsov, N.G. SERS-based lateral flow immunoassay of troponin I by using gap enhanced Raman tags. *Nano Res.* **2019**, *12*, 413–420. [CrossRef]
16. Yu, Q.; Wang, Y.; Mei, R.; Yin, Y.; You, J.; Chen, L. Polystyrene encapsulated SERS tags as promising standard tools: Simple and universal in synthesis; highly sensitive and ultrastable for bioimaging. *Anal. Chem.* **2019**, *91*, 5270–5277. [CrossRef]
17. Xie, L.; Lu, J.; Liu, T.; Chen, G.; Liu, G.; Ren, B.; Tian, Z. Key role of direct adsorption on SERS sensitivity: Synergistic effect among target, aggregating agent, and surface with Au or Ag colloid as surface-enhanced Raman spectroscopy substrate. *J. Phys. Chem. Lett.* **2020**, *11*, 1022–1029. [CrossRef]
18. Zhu, R.; Feng, H.; Li, Q.; Su, L.; Fu, Q.; Li, J.; Song, J.; Yang, H. Asymmetric core-shell gold nanoparticles and controllable assemblies for SERS ratiometric detection of microRNA. *Angew. Chem. Int. Ed.* **2021**, *60*, 12560–12568. [CrossRef]
19. Rodríguez-Lorenzo, L.; Álvarez-Puebla, R.A.; Pastoriza-Santos, I.; Mazzucco, S.; Stéphan, O.; Kociak, M.; Liz-Marzán, L.M.; de Abajo, G.F.J. Zeptomol detection through controlled ultrasensitive surface-enhanced Raman scattering. *J. Am. Chem. Soc.* **2009**, *131*, 4616–4618. [CrossRef]
20. Jain, P.K.; Huang, W.; El-Sayed, M.A. On the universal scaling behavior of the distance decay of plasmon coupling in metal nanoparticle pairs: A plasmon ruler equation. *Nano Lett.* **2007**, *7*, 2080–2088. [CrossRef]
21. Yan, B.; Thubagere, A.; Premasiri, W.R.; Ziegler, L.D.; Negro, L.D.; Reinhard, B.M. Engineered SERS substrates with multiscale signal enhancement: Nanoparticle cluster arrays. *ACS Nano* **2009**, *3*, 1190–1202. [CrossRef]
22. Pastorello, M.; Sigoli, F.A.; dos Santos, D.P.; Mazali, I.O. On the use of Au@Ag core-shell nanorods for SERS detection of Thiram diluted solutions. *Spectrochim. Acta Part A Mol. Biomol. Spectrosc.* **2020**, *231*, 118113. [CrossRef] [PubMed]
23. Lai, Y.; Dong, L.; Liu, R.; Lu, S.; He, Z.; Shan, W.; Geng, F.; Cai, Y.; Liu, J. Synthesis of highly-branched Au@AgPd core/shell nanoflowers for in situ SERS monitoring of catalytic reactions. *Chin. Chem. Lett.* **2020**, *31*, 2437–2441. [CrossRef]
24. Gu, W.; Zhao, Y.; Zhuang, S.; Zha, J.; Dong, J.; You, Q.; Gan, Z.; Xia, N.; Li, J.; Deng, H.; et al. Unravelling the structure of a medium-sized metalloid gold nanocluster and its filming property. *Angew. Chem. Int. Ed.* **2021**, *60*, 11184–11189. [CrossRef] [PubMed]

25. Phung, V.-D.; Jung, W.-S.; Nguyen, T.-A.; Kim, J.-H.; Lee, S.-W. Reliable and quantitative SERS detection of dopamine levels in human blood plasma using a plasmonic Au/Ag nanocluster substrate. *Nanoscale* **2018**, *10*, 22493–22503. [CrossRef] [PubMed]
26. Kuttner, C.; Höller, R.P.M.; Quintanilla, M.; Schnepf, M.J.; Dulle, M.; Fery, A.; Liz-Marzán, L.M. SERS and plasmonic heating efficiency from anisotropic core/satellite superstructures. *Nanoscale* **2019**, *11*, 17655–17663. [CrossRef]
27. Zhang, L.; Wang, X.; Zhang, Y. Photocatalytic properties of silver nanospherical arrays driven by surface plasmons. *Chemosensors* **2021**, *9*, 336. [CrossRef]
28. Dang, H.; Park, S.; Wu, Y.; Choi, N.; Yang, J.; Lee, S.; Joo, S.; Chen, L.; Choo, J. Reproducible and sensitive plasmonic sensing platforms based on Au-nanoparticle-internalized nanodimpled substrates. *Adv. Funct. Mater.* **2021**, *31*, 2105703. [CrossRef]
29. Wang, C.; Wang, C.; Li, J.; Tu, Z.; Gu, B.; Wang, S. Ultrasensitive and multiplex detection of four pathogenic bacteria on a bi-channel lateral flow immunoassay strip with three-dimensional membrane-like SERS nanostickers. *Biosens. Bioelectron.* **2022**, *214*, 114525. [CrossRef]
30. Ding, Q.; Wang, J.; Chen, X.; Liu, H.; Li, Q.; Wang, Y.; Yang, S. Quantitative and sensitive SERS platform with analyte enrichment and filtration function. *Nano Lett.* **2020**, *20*, 7304–7312. [CrossRef]
31. Bertok, T.; Bertokova, A.; Hroncekova, S.; Chocholova, E.; Svecova, N.; Lorencova, L.; Kasak, P.; Tkac, J. Novel prostate cancer biomarkers: Aetiology, clinical performance and sensing applications. *Chemosensors* **2021**, *9*, 205. [CrossRef]
32. Huang, Q.; Hu, Z.; Guo, S.; Guo, D.; Wang, R. Coupling an artificial receptor with macrophage membrane for targeted and synergistic treatment of cholestasis. *Supramol. Mater.* **2022**, *1*, 100020.
33. Qiao, N.; Zheng, J. Nonenzymatic glucose sensor based on glassy carbon electrode modified with a nanocomposite composed of nickel hydroxide and graphene. *Microchim. Acta* **2012**, *177*, 103–109. [CrossRef]
34. Sarma, T.K.; Chowdhury, D.; Paul, A.; Chattopadhyay, A. Synthesis of Au nanoparticle–conductive polyaniline composite using H_2O_2 as oxidising as well as reducing agent. *Chem. Commun.* **2002**, *10*, 1048–1049. [CrossRef] [PubMed]
35. Yan, X.; Jiang, M.; Hu, Y.; Wu, L.; Zhao, K.; Xue, X.; Zheng, X. A new chemiluminescence method for the determination of 8-hydroxyguanine based on L-histidine bound nickel nanoparticles. *Chem. Commun.* **2020**, *56*, 6535–6538. [CrossRef]
36. Qi, X.; Su, G.; Bo, G.; Cao, L.; Liu, W. Synthesis of NiO and NiO/TiO_2 films with electrochromic and photocatalytic activities. *Surf. Coat. Technol.* **2015**, *272*, 79–85. [CrossRef]